

NUMERICAL SIMULATION OF REAL VS THEORETICAL SPIRAL INFLECTOR

D.V. Altiparmakov and P. Beličev

VINČA Institute of Nuclear Sciences, P.O.Box 522, 11001 Belgrade, Yugoslavia

A comparison between the numerical and analytical computations of the electric field in the spiral inflector is presented in this paper. Stochastic beam simulation is carried out in order to clarify the effects. Both approaches lead to the same results when the radial emittance is considered. However, a remarkable difference is obtained in the case of axial emittance. Moreover, the longitudinal emittances differ drastically. This is mainly due to the v -component of the fringe field which is usually neglected in the analytical approaches.

1 Introduction

Quite a number of papers have treated the spiral inflector, since Belmont and Pabot [1] published their well known article on that subject. Two approaches to electric field computation have been used throughout these papers: (i) numerical field mapping and (ii) analytical field approximation. The former usually relies on a 3D solver of the Laplace equation, such as RELAX3D [2], while the latter applies some analytical expansions according to the curved surfaces of the inflector electrodes [3]. Both of them are implemented into the CASINO code [4] which is a widely used tool for inflector analysis. The intention of this paper is to present a comparison between these two approaches. The same subject has been already considered in Ref. [5] where a very well agreement of the two methods has been reported. However, our results are quite different, as shown in the last section of this paper.

1.1 Central trajectory and optical coordinate systems

The role of the spiral inflector is to bend the beam for 90° from the axial direction onto the median plane of the cyclotron. To achieve that, the shape of its electrodes must be designed so that the central trajectory obeys the well known equations that can be cast in the following form:

$$\begin{aligned} x_c &= \lambda(1 - \sin k\theta \sin \theta - \cos k\theta \cos \theta) \\ y_c &= \lambda(\sin k\theta \cos \theta - \cos k\theta \sin \theta) \\ z_c &= A(\sin \theta - 1) \end{aligned} \quad , \quad \begin{aligned} k &= A/R_m + k' \\ \lambda &= A/(k^2 - 1) \end{aligned} \quad (1)$$

where θ is the angle of inflection that varies from 0 (inflector entrance) to $\pi/2$ (inflector exit), A is the electric radius, R_m is the magnetic radius and k' is the tilt parameter. The above equations assume that the inflector exit is in the median plane ($z = 0$), while the inflector entrance is in x-y plane at the distance $z = -A$. One has to mention here that the above definition of the inflector parameter k differs for factor 2 from its usual definition.

In the analysis of the spiral inflector it is common practice to introduce an optical coordinate system (u, h, v) that travels along the central trajectory (x_c, y_c, z_c). The direction v coincides with the central particle velocity,

$$\vec{e}_v = \frac{\dot{x}_c \vec{i} + \dot{y}_c \vec{j} + \dot{z}_c \vec{k}}{\sqrt{\dot{x}_c^2 + \dot{y}_c^2 + \dot{z}_c^2}} = -\vec{i} \cos k\theta \sin \theta + \vec{j} \sin k\theta \sin \theta + \vec{k} \cos \theta \quad (2)$$

h is normal to v and lies in x-y plane,

$$\vec{e}_h = \frac{\dot{y}_c \vec{j} - \dot{x}_c \vec{i}}{\sqrt{\dot{x}_c^2 + \dot{y}_c^2 + \dot{z}_c^2}} = \vec{i} \sin k\theta + \vec{j} \cos k\theta \quad (3)$$

and u is the direction of the electric field defined as:

$$\vec{e}_u = \vec{e}_h \times \vec{e}_v \quad (4)$$

The vectors $(\vec{i}, \vec{j}, \vec{k})$ and $(\vec{e}_u, \vec{e}_h, \vec{e}_v)$ are the unit vectors of the axes (x, y, z) and (u, h, v) respectively, and the dot denotes the time derivative.

The above coordinate transformation can be presented in the following matrix form from which it is easy to see that it consists of two consecutive rotations: one around the z axis and the other around the y axis.

$$\begin{pmatrix} \vec{e}_u \\ \vec{e}_h \\ \vec{e}_v \end{pmatrix} = \begin{pmatrix} \cos \theta & 0 & \sin \theta \\ 0 & 1 & 0 \\ -\sin \theta & 0 & \cos \theta \end{pmatrix} \cdot \begin{pmatrix} \cos k\theta & -\sin k\theta & 0 \\ \sin k\theta & \cos k\theta & 0 \\ 0 & 0 & 1 \end{pmatrix} \cdot \begin{pmatrix} \vec{i} \\ \vec{j} \\ \vec{k} \end{pmatrix} \quad (5)$$

When a tilted inflector is considered, however, Eq. (5) is not sufficient. In that case it is useful to define an additional local coordinate system by rotation of u - h plane around the v axis for an angle ξ , i.e.

$$\begin{pmatrix} \vec{e}_u^r \\ \vec{e}_h^r \\ \vec{e}_v \end{pmatrix} = \begin{pmatrix} \cos \xi & -\sin \xi & 0 \\ \sin \xi & \cos \xi & 0 \\ 0 & 0 & 1 \end{pmatrix} \cdot \begin{pmatrix} \vec{e}_u \\ \vec{e}_h \\ \vec{e}_v \end{pmatrix}, \quad \xi = \arctg\left(k' \frac{A+z}{A}\right) \quad (6)$$

Now, the electric field is in the direction \vec{e}_u^r . Its u component bends the particle trajectory in vertical plane, while the h component is analogous to the magnetic field. However, the former is no longer constant due to the tilt.

To get a constant value, the electrode gap d must follow the variation of $\cos \xi$, i.e.

$$d = \frac{d_0}{\sqrt{1 + (k' \sin \theta)^2}} \quad (7)$$

where d_0 is the gap at the inflector entrance.

2 Inflector model and electric field computation

2.1 Numerical computation of the electric field

The inner surfaces of the electrodes represent actually two ruling surfaces. They can be specified [6] by two parallel lines that rule around the central trajectory at the distance $u = \pm d/2$. In the computations here presented we rather applied a solid modeling method instead to cope with such complex surfaces. There are two advantages of this approach: (i) one can use well developed CAD methods, and (ii) the complex shape of both the inflector and the housing can be easily specified.

The electrode gap can be represented as a union of a number of infinite cylinders of radius $d/2$ whose axes are in \vec{e}_u^r direction along the central trajectory. Then, to get the electrodes, this gap should be subtracted from a spatial domain that represents the inflector body. It is worthwhile to mention here that the inflector machining is usually done in that way. The infinite cylinder actually represents the bore made by the drilling machine.

To do the solid modeling we applied the RFG subroutine package [7,8]. The electrode gap is modeled by 60 cylinders (1.5° degrees of inflection). The inflector body (a kidney shaped spatial domain) is represented by 9 primitives, while 10-20 primitives are needed to model the housing depending on its actual shape. When the solid model is specified, the boundary condition problem of the Laplace solver reduces to the point inclusion problem.

To compute the electric potential we applied an over-relaxation finite difference method similar to RELAX3D. The calculations have been carried out on a mesh of $153 \times 181 \times 203$ grids with 0.25mm cell width size that results in ~ 5.6 millions of points. The typical computing time is 1-2 hours on a Pentium PC computer running on 166 MHz. When the electric potential map is computed, the calculation of electric field is performed by 5 points numerical differentiation.

2.2 Analytical approximation of the electric field

To this end we applied the formalism of the CASINO code. The first order expansion from Ref. [5] is used in order to calculate the field variation inside the inflector. This rather complicated formula can be simply expressed as follows,

$$\Delta \vec{E} = \frac{E_0}{A \cos \xi} \left[\cos \theta (\vec{G} \times \Delta \vec{r}) - (1 + k' \sin^2 \theta) (\Delta \vec{r} - \vec{h}_r) \right] \quad (8)$$

where $\Delta \vec{E}$ is the variation of the electric field, E_0 is the nominal field intensity, $\Delta \vec{r}$ is the displacement from the central trajectory, and the vector \vec{G} has the following form.

$$\vec{G} = - \left(k' \cos \xi + \frac{k}{\cos \xi} \right) \vec{e}_u^r + k' \sin \xi \vec{e}_h^r \quad (9)$$

It is assumed that the fringe field lies solely in the \vec{e}_u^r direction. Its magnitude is computed similarly to the CASINO code by the following formula

$$E = \frac{E_{ct}}{2} \left[1 + \tanh(\alpha (\pm (s - s_e - g) / g + \delta)) \right] \quad (10)$$

where s is the path length along central trajectory, s_e is the location of the inflector entrance (or exit), g is the distance between the inflector and the grounded screening electrode, and the constants α and δ are taken from CASINO, i.e.

$$\delta = 2.794 - e^{\frac{1.12 - g/d}{1.077}}, \quad \alpha = \frac{0.811}{\delta - 0.641} \quad (11)$$

3 Results of numerical simulation

3.1 Inflector parameters

In order to clarify the effects of the two methods of electric field computation we considered a spiral inflector with the following parameters:

Table 1: Inflector parameters

| Parameter | Value |
|-----------------------------|-----------------|
| Magnetic radius R_m | 18.2 mm |
| Electric radius A | 25.0 mm |
| Tilt k' | -0.44 |
| Inflector parameter k | 0.9336 |
| Maximal electrode gap d_0 | 7 mm |
| Electrode voltage V | ± 8.0836 kV |

This is one of the deflectors which is going to be used in the VINCY Cyclotron [9]. Therefore, the inflector housing is specified by the central region of this cyclotron.

3.2 Inflector models

In order to get an insight into the electric field effects, six inflector models have been considered:

- (1) Ideal inflector (the field off the central trajectory is equal to the field on it, with no fringe field).
- (2) Analytical model of the electric field according to Eqs. (8) to (11).
- (3) Numerical model that considers only the inflector electrodes in free space.
- (4) Numerical model that includes the inflector housing.
- (5) Numerical model that includes both the housing and two grounded electrodes (at the entrance and the exit) with a cylindrical hole of 6 mm diameter. The distance g between the inflector and the grounded electrodes is 5 mm.
- (6) The same as the previous one, but the distance g is decreased to 2 mm.

Figure 1 presents both u and h components of the electric field computed at the points $u=1\text{mm}$ and $h=2\text{mm}$ off the central trajectory. From the results of the numerical models one can see that the fringe field increases with the increase of g . The value $g=2\text{mm}$ is adopted as the minimum one that satisfies the Kilpatrick criterion [10]. The results show a good agreement between the analytical approximation and the numerical solution for the realistic inflector model ($g=2\text{mm}$).

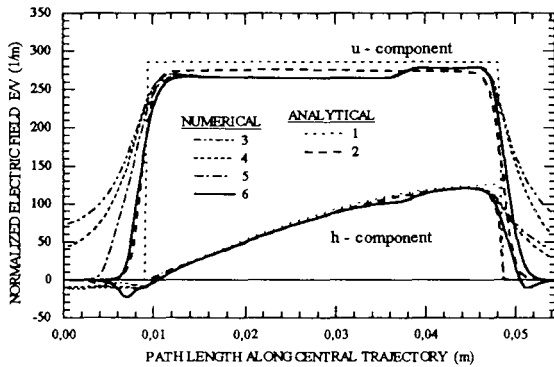


Figure 1: Electric field for different inflector models

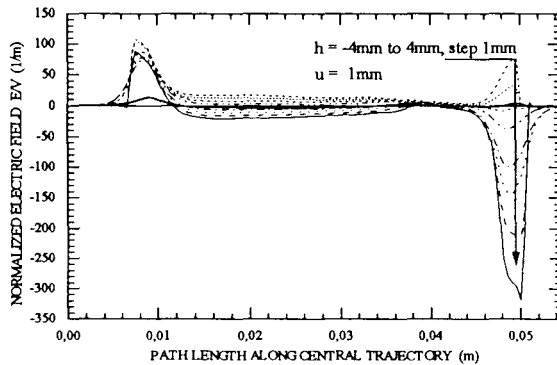


Figure 2: v component of the electric field

Figure 2 presents the v component of the electric field in the case of the realistic inflector model. The results are computed in the points $u=1\text{mm}$ and $h=-4\text{mm}$ to 4mm . One

can notice a very large variation of the fringe field. Taking into account that this component is neglected in the analytical approach, one may expect significant effect on the beam behavior.

3.3 Numerical beam simulation

Stochastic beam simulation is carried out for all the six models. Monoenergetic and continuous beam with Gaussian distribution has been considered. 80π mm-mrad uncorrelated emittances have been assumed in both transverse planes 9 mm before the inflector entrance. The output emittances have been calculated 20^0 after the inflector exit.

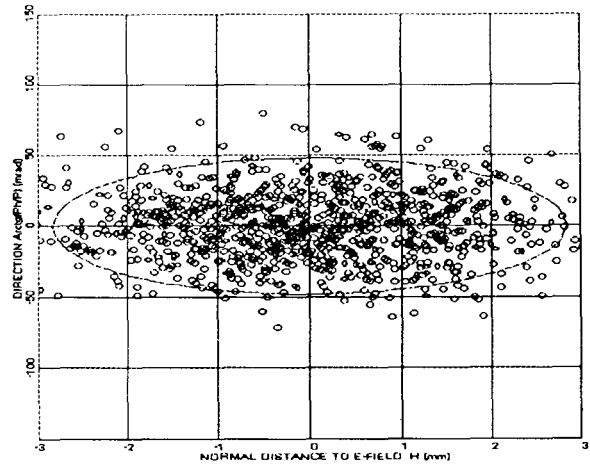


Figure 3: Radial output emittance for the analytical model

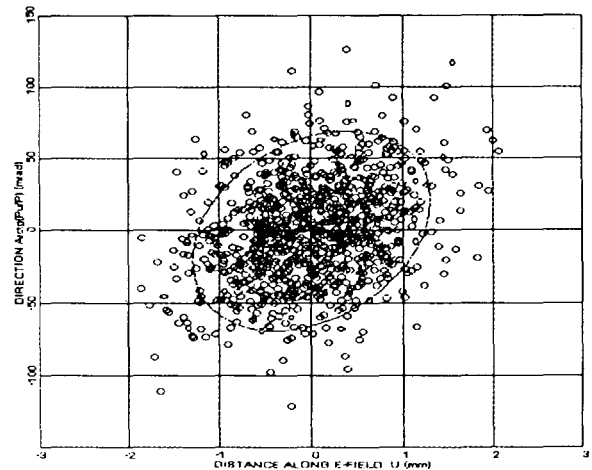


Figure 4: Axial output emittance for the analytical model

Figures 3 to 5 show the radial, axial and longitudinal output emittances, respectively, in the case of analytical approximation. The analogous results for the realistic inflector model are given in figures 6 to 8. For both models, almost no differences can be observed in the case of radial emittances. However, a remarkable difference can be seen

in the case of axial emittances. Moreover, the longitudinal emittances differ drastically. This is mainly due to the v component of the fringe field.

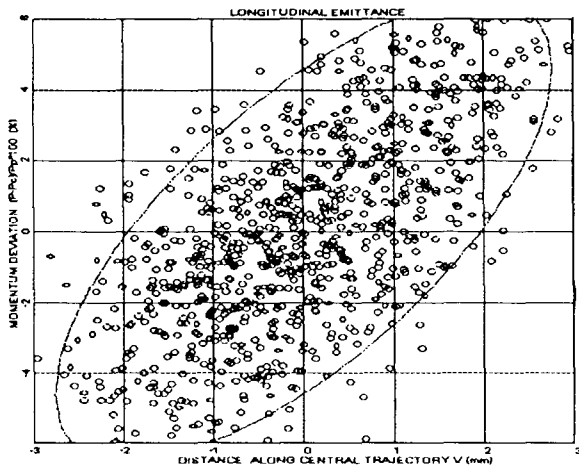


Figure 5: Longitudinal output emittance for the analytical model

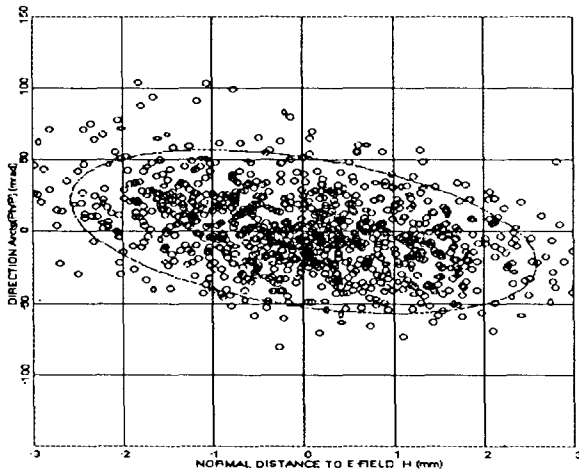


Figure 6: Radial output emittance for the realistic inflector model

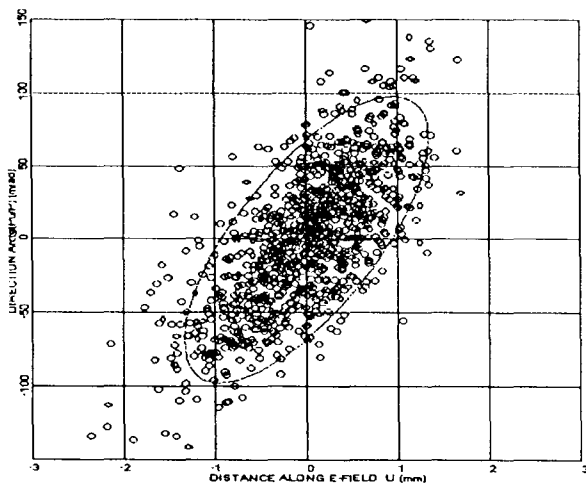


Figure 7: Axial output emittance for the realistic inflector model

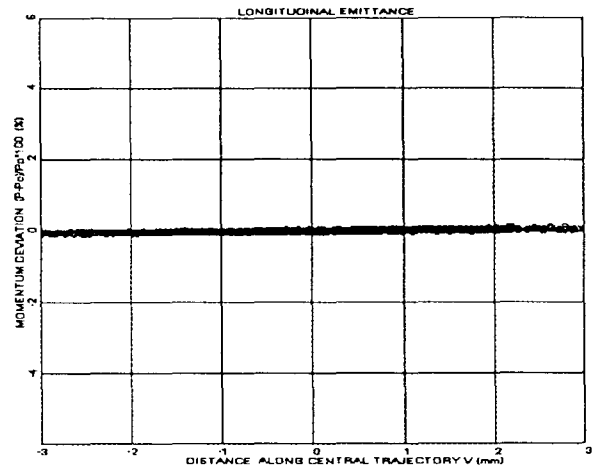


Figure 8: Longitudinal output emittance for the realistic inflector model

Conclusion

The difference between the analytical and the realistic inflector models implies that for an axial injection to cyclotron central region detailed matching calculation, the usage of numerically calculated electric field is of great importance. Further analysis of this type for different inflector parameters is necessary to reveal the range of validity of the obtained results.

References

- [1] J.L. Belmont and J.L. Pabot, *IEEE Trans. Nucl. Sci.*, NS-13, 191 (1966).
- [2] C.J. Kost and F.W. Jones, RELAX3D User's Guide and Reference Manual, TRI-CD-88-01 (1992).
- [3] L.W. Root, *Ph.D. Thesis, Univ. of British Columbia* (1972).
- [4] B.F. Milton and J.B. Pearson, CASINO User's Guide and Reference Manual, TRI-DN-89-19 (1993).
- [5] R.J. Balden et al., Aspects of Phase Space Dynamics in Spiral Inflectors, in *Proc. 12th Int. Conf. On Cyclotrons and their Applications*, pp. 435-438 (1989)
- [6] Lj. Milinković, RELAX3D Spiral Inflectors, TR30-DN-89-21 (1989).
- [7] D.V. Altiparmakov and P. Beličev, *Prog. In Nucl. Energy*, 24, pp. 77-88 (1991)
- [8] D.V. Altiparmakov RFG Subroutine Package for Solid Modeling and Ray/Solid Intersection, Belgrade (1996)
- [9] W.D. Kilpatrick, *Review of Sci. Instruments*, 28, pp. 824-826 (1957).
- [10] D.V. Altiparmakov and P. Beličev, Spiral Inflector of the VINCY Cyclotron, in *Proc. 12th Information Meeting on the TESLA Accelerator Installation*, Belgrade (1997).